How can power-to-ammonia be robust? Optimization of an ammonia synthesis plant powered by a wind turbine considering operational uncertainties.

Kevin Verleysen[a,b,*], Diederik Coppitters[a,b,c], Alessandro Parente[b], Ward De Paepe[c], Francesco Contino[a,b],

[a] *Vrije Universiteit Brussel (VUB), Thermo and Fluid dynamics (FLOW), Pleinlaan 2, 1050 Brussels, Belgium*
[b] *Vrije Universiteit Brussel (VUB) and Université Libre de Bruxelles (ULB), Combustion and Robust Optimization Group (BURN), 1050 Brussels, Belgium*
[c] *University of Mons (UMONS), Thermal Engineering and Combustion Unit, Place du parc 20, 7000 Mons, Belgium*

Abstract

The increasing share of wind energy induces a strain on the electricity network. To unburden the transmission system operators from this strain, the dispensable wind energy can locally be stored in an energy carrier, e.g. ammonia (NH_3). Existing work considers fixed operational parameters during design optimization to represent real-life conditions of the Power-to-NH_3 system. However, uncertainties significantly affect real-life performances, which can lead to suboptimal plants. To provide a robust design—least sensitive to uncertainties—we considered the main operational uncertainties during design optimization and illustrated the contribution of each uncertainty on the systems NH_3 production. This work presents the optimization under uncertainty of the Power-to-NH_3 process and a global sensitivity analysis

*Corresponding author
Email address: kevin.verleysen@vub.ac.be (Kevin Verleysen)

on the optimized designs. The results revealed a design trade-off, where a *productive* design produces 3.2 times more NH_3 on average, but is 2.6 times less robust (higher standard deviation) than the *robust* design. A global sensitivity analysis on the most robust design showed that the temperature fluctuation of the NH_3 reactor dominates the average NH_3 production by 99.7%. The same sensitivity analysis on the most productive design showed that the wind speed measurement error and the temperature variation are both influencing the ammonia production by respectively 75.4% and 22.5%. Accordingly, an accurate anemometer and improving the temperature control over the NH_3 reactor are the most effective actions to make the most productive design more robust. However, a robust plant can be obtained by decreasing the load size of the plant. It suffices to improve the temperature control over the NH_3 reactor to make this design (adopted from the trade-off) less sensitive to the noise. Future investigations involve analyzing the dynamic operations of the robust Power-to-NH_3 pathway and analyze the impact of uncertainties on its levelized cost.

Keywords: Power-to-ammonia, Robust design optimization, Haber-Bosch synthesis, Seasonal hydrogen storage, Energy storage system

---

1. Introduction

The erratic nature of renewable sources requires a higher degree of flexibility of the electricity grid [1]. To avoid this requirement, an energy storage system is necessary to regulate the supply of this non-dispatchable energy, removing its intermittent effect on the grid. The primary purpose of the storage system is to capture the excess energy at any time and inject it back into the network to compensate for variability between supply and demand without relying on fossil fuels while improving the security of electricity supply in a sustainable way [2, 3]. For significant power levels, the production of chemicals can be employed to store the energy in an electrochemical energy carrier. This energy carrier could subsequently fuel a power production system for power generation; balancing the electricity network for prolonged power disruptions and reducing the need for a flexible grid [4].

The hydrogen-based Power-to-Power (PtP) concept enables the storage of large-scale (up to GW) power via water electrolysis, but realizing it in practice is proven difficult. Still, the declining cost in renewable technologies promoted the creation of numerous research and demonstration projects across Europe [5–8]. However, storing pure H_2 in a compressed or cryogenic (below -253°C) container for several months provides low PtP efficiencies (between 34% and 38%) and includes higher storage costs [9]. Besides, the storage of this substance introduces safety issues due to its invisible, odorless and flavorless properties, making it hard to detect leaks and increases the risk of explosion [10, 11].

A more viable and safer way for the implementation of this hydrogen-based energy storage system is by converting the electrolytic H_2 to ammonia (NH_3), using the industrially mature Haber-Bosch Synthesis (HBS) process [12]. The HBS process consists of synthesizing a mixture of H_2 and nitrogen gas (N_2) to form NH_3 in the presence of a catalyst at an operational temperature between 350°C and 550°C and a pressure ranging from 150 bar to 250 bar [13–15].

NH_3 gained a significant role during recent years in the application of large-scale H_2 storage, but also for its potential utilization as a maritime fuel and sustainable nitrogen-based fertilizer [16–20]. Morgan et al. [13] developed an analytic model to determine in which circumstances this Power-to-Ammonia (PtA) concept can be economically viable in addition to a diesel-fueled generator for a geographic islanded case. A more extensive analysis by Bañares-Alcántara et al. investigated the potential use of NH_3-based energy storage in electric islanded cases [14]. Later on, the Institute for Sustainable Process Technology (ISPT) presented a feasibility study for implementing this renewable NH_3 concept of storing the abundance of wind energy for local farming and power generation in the Netherlands by considering economic and industrial competitive scenarios [9]. The studies of Sánchez et al. [21, 22] investigated the optimal scaling of each subprocess (differentiating between air separation units and ammonia synthesis reactors), providing a relation between NH_3 production and investment cost linked to the renewable energy supply mix to the PtA plant. The studies carried out by Allman et al. [23], Beerbühl et al. [24] and Palys et al. [25] incorporated the capacity sizing and energy scheduling of the PtA plant, while considering the variability of solar and wind energy into the design optimization. Pilot plants of such an ammonia-based energy storage system are built in two locations in the world, namely at the Rutherford Appleton Laboratory (RAL) in the UK and the Fukushima Renewable Energy Institute - AIST (FREA) in Japan. The goal of the PtA plant at RAL is improving the plants' commercial possibilities for providing a market-flexible energy carrier [18], while the research objective of the demonstration plant at FREA is to enhance the HBS process with the development of new Ruthenium catalysts, which enables the NH_3

synthesis at a low-pressure and low-temperature environment [26]. The presence of uncertainties is however observed by Reese et al. on the operations of a small-scale ammonia synthesis pilot plant located in Minnesota in the form of temperature and pressure fluctuations in the reactor [17]. Although each study included a sensitivity analysis of the electrolyzer's operation and the HBS process, no investigation has been done on the identification and quantification of operational uncertainties influencing the performance of the entire storage system.

This paper provides the modeling of the NH_3-based energy storage together with the identification of reported operational uncertainties from literature, which was combined to perform a design optimization under uncertainty. We performed the modeling of an electrolyzer operating with an alkaline electrolyte, a Pressure Swing Adsorption (PSA) to obtain nitrogen from the air, and a Haber-Bosch Synthesis (HBS) plant to synthesize NH_3 in Aspen Plus. In addition to the chemical modeling in Aspen Plus, a Wind Turbine Generator (WTG) is created in Python to convert wind speed into electric power. These models were assembled and optimized with a Multi-Objective Genetic Algorithm (MOGA) to establish a set of optimized designs. This energy model was then combined with the identified operational uncertainties of each subsystem to establish an optimization under uncertainty by the use of an Uncertainty Quantification (UQ) algorithm. With the MOGA and UQ approach, a set of optimized designs was determined, which were least sensitive to the effect of these uncertainties while maximizing the NH_3 production. This so-called Robust Design Optimization (RDO) approach improves the design of the plant in the presence of parametric uncertainties.

The RDO process consisted of combining the Nondominated Sorting Genetic Algorithm (NSGA-II) [27] and the Polynomial Chaos Expansion (PCE) technique [28], which ultimately evolved the defined decision variables towards a better performance while taking into account the implemented uncertainties.

2. Modeling the storage of wind energy through ammonia synthesis

This section presents the design of each process necessary to store wind energy in the energy carrier NH_3. The first subsection provides the wind speed data used to power the storage system. This power is determined by the model of a wind turbine in Python. Each following subsection presents the modeling of an Alkaline Water Electrolyzer (AWE), a PSA and the HBS in Aspen Plus. The description and integration of the operational uncertainties are included for the wind turbine model, the AWE and the HBS at each corresponding subsection.

2.1. Wind power generation

We incorporated the hourly wind speed measurement data of a wind turbine park located in Galicia (Spain) and sequentially sorted the data in a wind speed frequency distribution with a step size of 1 m/s [29]. Through the integration of a power curve of a typical wind turbine model, this wind speed data is converted into electric power. We based this power curve on the design of the Vestas V112 onshore wind turbine and integrated this curve in Python through Equation 1 to calculate the generated wind power (P_{WTG}):

$$P_{\mathrm{WTG}} = \frac{1}{2}\rho A C_P v^3 \qquad [\mathrm{W}], \tag{1}$$

where ρ is the density of air in kg/m^3 (at sea level and at 15°C, ρ = 1.22 kg/m^3), A is the area of the rotating blades in m^2, C_P is the power coefficient and v is the wind speed in m/s.

In the adopted model, the maximum power output was adjusted to 3 MW at a rated wind speed of 11 m/s while assuming a constant power coefficient of 37%. We performed this adaptation to correlate the wind speed and electric power between the cut-in and rated wind speed with the cubic relationship (Equation 1) without considering the dependency of C_p on the wind speed. The original and adopted design specification are provided in Table 1.

Table 1: Wind turbine generator design specifications, constraints and wind speed measurement uncertainty.

Design specification		Reported value [30]	Adopted value
C_P	[W/W]	$C_P(v)$	37.0
A	[m^2]	9852.0	9852.0
Constraints			
$v_{\text{cut-in}}$	[m/s]	3	3
v_{rated}	[m/s]	12	11
$v_{\text{cut-out}}$	[m/s]	25	25
Uncertainty		Integrated value [31]	
$e_{\text{measurement}}$	[-]	±1%	

Wind turbines are inherently influenced by a variety of uncertainties, providing ambiguous prospects for start-up wind turbine parks. These uncertainties have a direct effect on the profitability of these projects, which are mainly based on wind speed measurements or estimations to forecast the capacity factor [32] or the Annual Energy Production (AEP) of a location [33]. Lackner et al. categorized a variety of uncertainties influencing this AEP in four categories, which consists of: wind speed measurement uncertainty, historical wind speed data, wind resource modeling variability, and lastly, the site assessment uncertainty [33]. Because the wind speed measurements for one year are used in this design optimization study (not the power production of an actual wind turbine), only the first category of Lackner et al. (the wind speed measurement error) is applied to the design of the WTG and considered in the UQ analysis. Kaganov et al. designated the wind speed measurement error of rotational measurement devices between 1% and 6% [31]. We integrated a wind speed measurement uncertainty of 1% to consider the most accurate wind speed measurement in the wind turbine design. A Gaussian distribution characterizes this uncertainty in the UQ analysis because the real distribution of the wind speed measurement error is unknown in this context [33]. The UQ analysis assesses the uncertainty propagation for each design on the considered objective. The following expression enables the implementation of this uncertainty (Equation 2):

$$v_{\text{measurement}} = v_{\text{data}}(1 - e_{\text{measurement}}) \qquad [\text{m/s}], \tag{2}$$

where $v_{\text{measurement}}$ is the measured wind speed in m/s resulting from the input wind data (v_{data}) and the error of the device ($e_{\text{measurement}}$) in %. During the robust design optimization process, the measured wind speed ($v_{\text{measurement}}$) replaces the wind speed (v) in Equation 1.

2.2. Alkaline water electrolyzer

An Alkaline Water Electrolyzer (AWE) was selected because of its proven reliability in industrial applications and a multitude of commercially available technologies on the market, allowing the AWE to operate commercially at MW scale [15, 34, 35]. The AWE process was modeled in Aspen Plus for one electrolytic cell (Figure 1). To resemble the real operation of an AWE and determine the hydrogen production when applying electric power to the electrolyzer stack, the electrolyzer model of Ulleberg [36] is integrated with a FORTRAN calculator in the 'Electrolytic cell' block (Figure 1). Ullebergs electrolyzer model consists of two empirical equations: a voltage-current (U-I) relationship and the characterization of the Faraday efficiency (η_{F}).

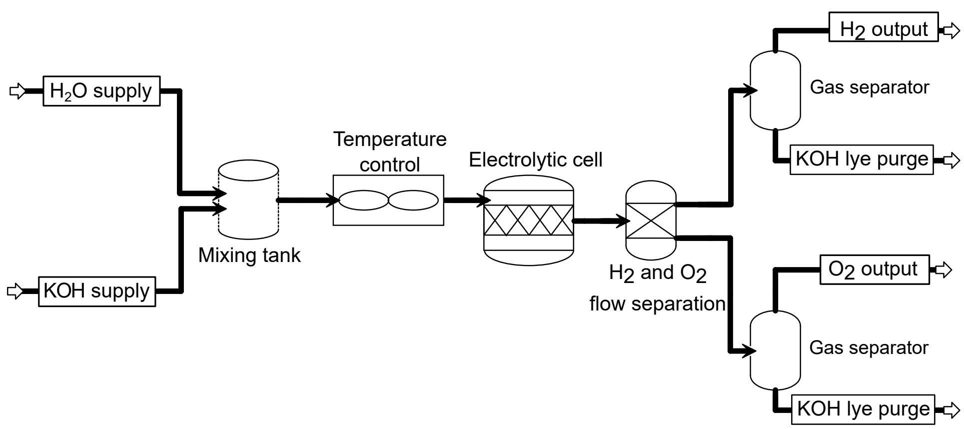

Figure 1: In the Aspen model of the electrolyzer, KOH lye dissolves in a tank with water, where its exothermic reaction increases the temperature of the mixture and is controlled by a heat exchanger before entering the electrolytic cell. The block components of one electrolytic cell and the product separation creates the H_2 and O_2 flows. The gas separation blocks separate the H_2 gas and KOH mixture.

The applied voltage U on the electrolytic cell is determined by the reversible voltage U_{rev} of the electrolytic reaction, the current I flowing through the electrolytic cell and T the operational temperature of the electrolytic cell. This relationship is defined with the following expression [36]:

$$\begin{aligned} U_{\mathrm{real}} =& U_{\mathrm{rev}} + (r_1 + r_2 T)\frac{I}{A} \\ &+ (s_1 + s_2 T + s_3 T^2)\log\Big((t_1 + t_2/T + t_3/T^2)\frac{I}{A} + 1\Big) \quad [\mathrm{V}], \end{aligned} \tag{3}$$

where r_i are the parameters related to the ohmic resistance of the electrolyte (for i = 1,2), s_i and t_i are the coefficients for overvoltage on the electrodes (for i = 1,2,3) and A the surface area of the electrodes in m^2. Ulleberg determined the value of these parameters (r_i, s_i and t_i) by a non-linear regression deterministic process (see Table A.5) [36].

Faraday's law determines the amount of hydrogen produced by the electrolyzer. This law states that the molar flow rate of the produced hydrogen ($\dot{n}_{\mathrm{H}_2}$) depends on the total number of electrolytic cells N and the transfer rate of electrons (Equation 4) [36]:

$$\dot{n}_{\mathrm{H}_2} = \eta_{\mathrm{F}}\frac{NI}{zF} \qquad [\mathrm{mol/s}], \tag{4}$$

where η_{F} is the Faraday efficiency of the electrolytic reaction. This Faraday efficiency expresses the ratio of the flow rate of hydrogen that is produced by the alkaline electrolyzer, over the theoretical production rate. This ratio is expressed by the second empirical formula with Equation 5 [36]:

$$\eta_{\mathrm{F}} = f_1 \exp\Big(\frac{f_2 + f_3 T}{I/A} + \frac{f_4 + f_5 T}{(I/A)^2}\Big) \qquad [-], \tag{5}$$

where f_i (for i = 1,...,5) are the parameters defining the evolution of the

Faraday efficiency, determined by the same non-linear regression process used in Equation 3 at an operational pressure of 7 bar (Table A.5) [36].

Mori et al. studied the steady-state operations of an alkaline electrolyzer, where a sinusoidal behavior of the cell temperature is observed. This temperature varied with a range of $\pm 3^o$C from the desired temperature [37]. The study acknowledged that the heat exchanger controlling the temperature causes this variation in temperature. When implementing this variation in the temperature control block of the AWE Aspen Plus model, the Faraday efficiency (Equation 5) and cell current (through the U-I relationship defined with Equation 3) are affected by this uncertainty, resulting in a variance of hydrogen production (Equation 4). This operational uncertainty is treated as a measurement error, affecting the control of the electrolytic cell temperature, which is included during the global sensitivity analysis and the robust design optimization within this study. Like the wind speed measurement error, the nature of the temperature measurement distribution is unknown, for which a Gaussian distribution is applied to the model. The UQ analysis assesses the effect of the variation of the cell temperature for each GA-generated design on the investigated output.

2.3. Pressure swing adsorption

The Pressure Swing Adsorption (PSA) process is selected to obtain nitrogen from the air. Frattini et al. proposed a simplified model of the PSA process in Aspen Plus, where the design incorporates a single-stage compressor, to pressurize the airflow (consisting of 75.5 wt% N_2), and a separation block, to obtain nitrogen [15]. The same philosophy has been used in Morgan et al. for a mathematical model of a wind-powered ammonia plant in steady-state operations [13]. The nitrogen production depended in both cases on the delivered power to the PSA compressor, which can be expressed with the following relationship between the power P_{PSA} and the air mass flow rate $\dot{m}_{\mathrm{air}}$ [13]:

$$P_{\mathrm{PSA}} = \frac{\dot{m}_{\mathrm{air}}}{\eta_{is}\eta_{\mathrm{mech}}}\Big(\frac{k}{k-1}\Big)T_{\mathrm{in}}R\left[\left[\frac{p_{\mathrm{out}}}{p_{\mathrm{in}}}\right]^{\frac{(k-1)}{k}} - 1\right] \qquad [\mathrm{W}], \tag{6}$$

where η_{is} is the isentropic efficiency ($\eta_{is} = 0.75$ [13]), η_{mech} the mechanical efficiency ($\eta_{\mathrm{mech}} = 0.95$ [13]), T_{in} the inlet temperature in K, R the gas constant of air in J/kgK, k the heat capacity ratio ($k = 1.4$), p_{out} the outlet pressure in bar ($p_{\mathrm{out}} = 7$ bar), and p_{in} the inlet pressure in bar ($p_{\mathrm{in}} = 1$ bar). The mass flow of air ($\dot{m}_{\mathrm{air}}$) is split into a pure mass flow of nitrogen and a residual flow of O_2 and Ar by a separation block in Aspen Plus. The compressor and separator block in Aspen Plus uses the PENG-ROB property method, which is based on the Peng-Robinson cubic equation of state [15].

2.4. Haber-Bosch synthesis process

An ammonia synthesis design is adopted from the paper of Frattini et al. to replicate the Haber-Bosch Synthesis (HBS) process performance [15]. In the first stage of modeling the ammonia process, the block specifications provided by the paper are implemented in Aspen Plus (Figure 2) [15]. In the subsequent step, we simplified the Haber-Bosch synthesis loop to reduce the computational cost while creating a single link between the generated wind power and the performance of the HBS process. This model reduction enabled us to govern the process by a single control parameter. To reach this necessary simplification, several adaptations were applied to the HBS loop of

Frattini et al. [15]. Frattini et al. initially integrated pressure losses through the use of the tube-and-shell designs in the integrated heat exchangers ((3) and (5) in Figure 2) [15]. These pressure losses were discarded from the model. Hence, the reactor compressor (6), which compensated for these pressure losses, could be excluded from the model. The model reduction resulted in the exclusion of the power consumption for this compressor. A second modification on the adopted model is the removal of the conditioning block (1), where water particles from the air or the electrolyzer are cleansed from the flow entering the synthesis loop (Figure 2). Because of the absence of water in both flows, we excluded this condition block from the model. We considered as well pure hydrogen and nitrogen flow rates from the AWE and PSA processes to avoid dealing with the catalyst poisoning caused by the presence of oxygen in both streams, which is a well-reported problem for iron-based catalysts [38]. In industrial processes, a purity of 99.9999% is required with the help of an additional purification system to overcome the deactivation of the ammonia synthesis catalyst [38].

These modifications resulted in the use of a single control parameter, namely the direct control over the operational pressure within the synthesis loop through the loop compressor ((2) in Figure 2). This loop compressor is sequentially governed by the power supply to this component, as is expressed with Equation 7 for a three-stage compressor.

$$P_{\mathrm{HBS}} = \frac{\dot{m}_{\mathrm{mix}}}{\eta_{is}\eta_{\mathrm{mech}}} \sum_{i=0}^{2} \left(\left(\frac{k}{k-1} \right) T_i R \left[\left[\frac{p_{i+1}}{p_i} \right]^{\frac{(k-1)}{k}} - 1 \right] \right) \qquad [\mathrm{W}] \qquad (7)$$

In this expression, P_{HBS} presents the delivered power to Haber-Bosch

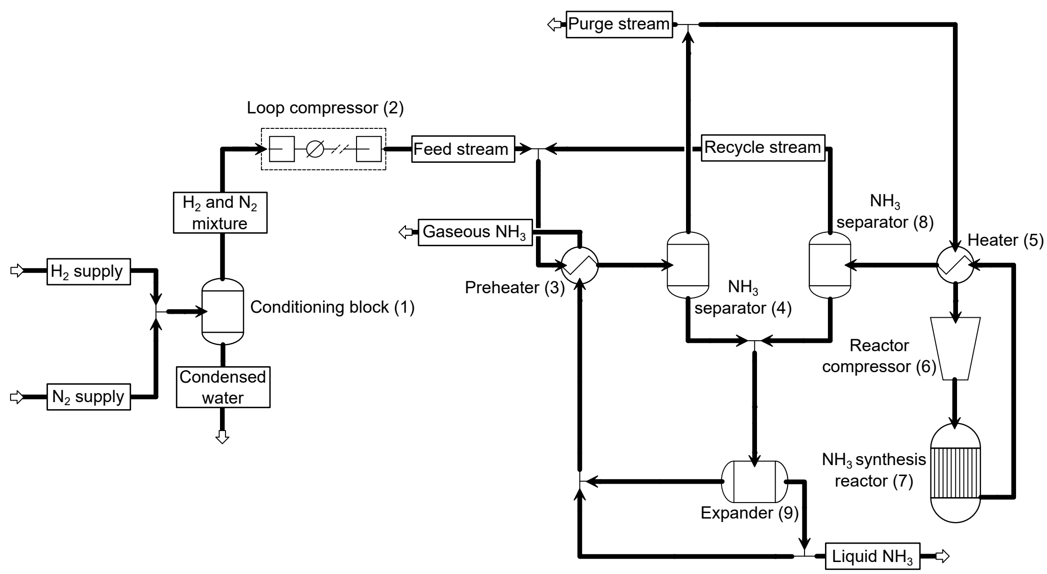

Figure 2: Frattini et al. modeled the Haber-Bosch Synthesis (HBS) loop in Aspen [15]. In this HBS, the loop compressor (2) pressurizes a mixture of H_2 and N_2, where the NH_3 synthesis reactor (7) converts this mixture to NH_3. The ammonia is extracted from the loop through condensation ((4), (8) and (9)).

compressor in W, $\dot{m}_{\text{mix}}$ the mass flow of gas mixture in kg/s, η_{is} isentropic efficiency, η_{mech} the mechanical efficiency, $T_{\text{in},i}$ inlet temperature of stage i in K (for $i = 0$ to 2), R the gas constant of mixture in J/kgK, k the heat capacity ratio, $p_{\text{in},i}$ the inlet pressure in kPa at stage i in kPa (for $i = 0$ to 2) and $p_{\text{out},i+1}$ the outlet pressure in kPa at stage i in kPa (for $i = 0$ to 2). Frattini et al. provided the decision variables of the loop compressor, which is modeled with an MCompr block in Aspen Plus based on the isentropic compressor model [15]. We compared the HBS power consumption of this simplified process to the described ammonia synthesis loop in the study of Morgan, where this study reported that 5.49% of the total power consumption of an ammonia plant goes to the ammonia synthesis loop [39]. In comparison with our modeled HBS loop, we observed that the loop compressor consumes 4.44% of the total power provided to the ammonia plant. This similar result proves that the applied simplifications are in agreement with another reported PtA energy model.

Operational uncertainties and instability phenomena in the ammonia synthesis process are described in the literature [17, 40]; therefore, disturbances are inherently present in this part of the energy storage model. The paper of Reese et al. acknowledged the presence of uncertainties in practice for a wind-powered ammonia synthesis plant [17]. Although the plant integrated a control system to govern the operations, the measurements of a three-day operation of this plant showed temperature and pressure fluctuations during the steady-state process. The paper interpreted this variability due to the undamped nitrogen supply of the PSA system and the occasional absence of hydrogen coming from the electrolysis process. However, these reported temperature fluctuations are essentially present during the operations and reach up to 50°C [17] without proper identification or analysis of disturbance. The mathematical model of an ammonia synthesis reactor and a heat exchanger of Jinasena et al. also showed temperature oscillations of this process where a temperature fluctuation of 10°C is present [40]. We included the same reactor temperature fluctuation of ±10°C with a Gaussian distribution within the proposed energy storage model. The cause of this variability is linked to the temperature measurement noise affecting the heat exchanger at the reactor inlet. For this reason, we chose the Gaussian distribution to represent this noise. This uncertainty is introduced into the operational temperature of the reactor (7) of the Aspen Plus model. Although pressure fluctuations were also reported in [17], these variations manifested due to erratic flow supply of hydrogen and nitrogen towards the synthesis process, where the origins of the temperature variations were unsubstantiated.

3. Optimization methodology

In this section, the optimization objectives are defined and discussed. The following two subsections designate the design search space and constraints to locate the global optimum within the model constraints. The final part of this section describes the applied MOGA to find these global optimum and the chosen UQ analysis, which collectively create the RDO approach. This approach is deemed necessary to maximize the performance of the plant while minimizing the sensitivity of the noise factors on this performance, i.e. robustifying the PtA process.

3.1. Optimization objective

The optimization objectives of this paper were chosen in function of the considered approach (deterministic or robust design optimization). In the Deterministic Design Optimization (DDO) process, the search algorithm maximizes the storage of wind energy while conceiving a design able to continuously operate, i.e. maximizing the plants' load factor, which provides a higher energy efficiency and ultimately achieve a better economic return on investment [41]. This load factor (L_F), chosen as the second objective, is expressed by the ratio of average consumed power over time (P_{average}) and the plants maximum consumed power ($P_{\text{plant,max}}$) and formulated with Equation 8:

$$L_F = \frac{\sum_{i=1}^{t} P_{\mathrm{plant}}(i)}{P_{\mathrm{plant,max}} t} = \frac{P_{\mathrm{average}}}{P_{\mathrm{plant,max}}} \qquad [-], \tag{8}$$

where P_{plant} is the power consumed by the total plant at a certain time in W and t the time in hours.

In the robust design optimization, the robustification of the ammonia production is opted as the final objective to make it less sensitive to the noise propagation incorporated in the subsystems. We focused on this objective to provide a design that can capture the highest amount of wind energy and store it through the production of the studied energy vector while being less influenced by operational uncertainties. This objective is split into two parts, where the average ammonia production needs to be maximized and, secondly, the sensitivity on the ammonia production is minimized. The ratio of the standards deviation (σ) over its average value (μ) of the concerned output characterizes this sensitivity, which is defined in literature as the Coefficient of Variance (CoV). This CoV is expressed in Equation 9 when applied on the ammonia production:

$$\mathrm{CoV} = \frac{\sigma_{\mathrm{NH_3}}}{\mu_{\mathrm{NH_3}}} \qquad [-]. \tag{9}$$

3.2. Design search space

The optimization method enhances the energy storage model according to a sorted wind speed data set (the design parameter) while finding the best performing plant design corresponding to the chosen objectives. This best performing design can be reached by searching the optimized set of decision variables within the defined search space. For attaining this optimized set, specific decision variables were selected to optimize the flow of power to each subsystem (AWE, PSA and HBS) according to the wind speed occurrence of the location in Galicia (Spain).

To control the amount of energy captured and converted by the ammonia plant, the simulation disposes of a part of the generated wind power by means of peak shaving; taking the total plant power size as the first decision variable ($\%_{\mathrm{plantsize}}$ in Figure 3). This captured power is then subdivided into three fractions, where a proportion of power is supplied to the AWE ($\%_{\mathrm{AlkalineWaterElectrolyzer}}$), another part to the PSA ($\%_{\mathrm{PressureSwingAdsorption}}$ and the residual power to the Haber-Bosch compressor to pressurize the ammonia synthesis process (Figure 3). To define the necessary decision variables and attain an optimized configuration, each subsystem generates hydrogen, nitrogen and ammonia at an individual flow rate. The power sizing of the AWE and PSA are therefore considered as the two successive decision variables, while the power supplied to the HBS compressor is employed as a control parameter (Figure 3). However, a single electrolytic cell can consume a maximum power of 2.1 kW [36], so the stack sizing of the electrolyzer has to be taken into account to predict the required installed capacity for a specific design. The number of electrolyzers (N) is therefore selected as the fourth and final decision variable. The candidates generated by the optimization algorithm for this decision variables have continuous values during the design optimization, allowing the GA to determine the electrolyzer capacity sizing (through the evaluation of the electrolyzer cells in series). In the discussion of the results (Section 4), these decision variable values were rounded up to the nearest integer, which provided a slightly higher annual ammonia production comparing when rounding this decision variable down (absolute difference of 0.01 tonne NH_3). For the load factor (L_F), these results were not altered by this design choice.

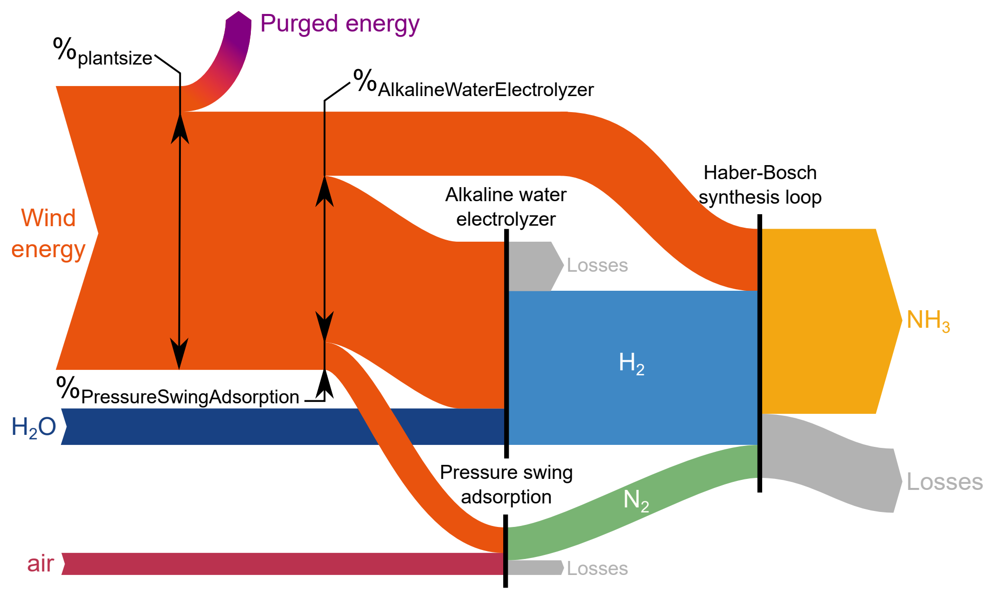

Figure 3: The wind turbine transforms the wind speed into electric power, which powers, according to a certain ratio, the electrolyzer, the air separation and the Haber-Bosch process. These processes produce H_2, N_2 and, finally, NH_3, respectively. The power ratio towards the individual processes, the plant load size and the numbers of electrolyzers are decision variables.

The design search space bounds each decision variable by a minimum and maximum value, so an optimized set of decision variables can be located (Table 2). For the plant sizing ($\%_{\text{plantsize}}$), the proportion of power flowing to the total ammonia plant can range between 0.001% and 100% according to the 3 MW power capacity of the WTG. This range allows the algorithm to decide which quantity of wind power can be captured by the NH_3 plant. The boundaries of the power proportion of the AWE and PSA ($\%_{\text{AWE}}$ and

$\%_{PSA}$) are selected based on a sensitivity analysis of the Aspen Plus model. The analysis shows that the proportion of power to the AWE varies between 91% and 95% at optimal/stoichiometric conditions (HBS loop pressure of 250 bar and a H_2/N_2 ratio of 3 mol/mol). For the PSA, this parameter varies between 0.9% and 1.6%. We chose a range from 1 to 2600 electrolytic cells to assure the ability of the AWE to perform at an operational power of 3 MW.

Table 2: Ranges of the decision variables (power allocation to the main and subprocesses, number of electrolyzer cells) chosen by the NSGA-II algorithm, where each design is assessed if none of the three model constraints are violated (Haber-Bosch loop pressure, H_2/N_2 ratio and current density for one electrolytic cell).

Decision variables		Range		Model constraints		Range	
		min	max			min	max
$\%_{plantsize}$	[%]	0.001	100	I/A	[mA/cm^2]	f($\eta_{thermal}$)	300
N	[-]	1	2600	p_{HBS}	[bar]	100	250
$\%_{AWE}$	[%]	91	95	H_2/N_2	[-]	1.5	4.5
$\%_{PSA}$	[%]	0.9	1.6				

3.3. Constraints

Based on the declared restraints by the manufacturer of the alkaline electrolyzer and safety regulations of the ammonia synthesis loop, we constrained three output parameters of the total energy storage model (Table 2). These three parameters are the current density of the electrolytic cell, the H_2/N_2 ratio entering the HBS compressor and its outlet pressure.

Each electrolytic cell is bounded by a maximum current density of 300 mA/cm^2 [36]. The minimum current density depends on the thermal efficiency (η_{thermal}) which is expressed by Equation 10:

$$\eta_{\text{thermal}} = \frac{U_{\text{tn}}}{U_{\text{real}}} \qquad [-] \tag{10}$$

where U_{tn} is the thermoneutral voltage in V [36].

When the thermal efficiency of the electrolytic cell is higher than 100%, the system requires heat to operate. Because the AWE is a low-temperature electrolyzer, the cell is unable to operate at this point; leading to the elimination of these decision variables from the set of solutions (Figure 4).

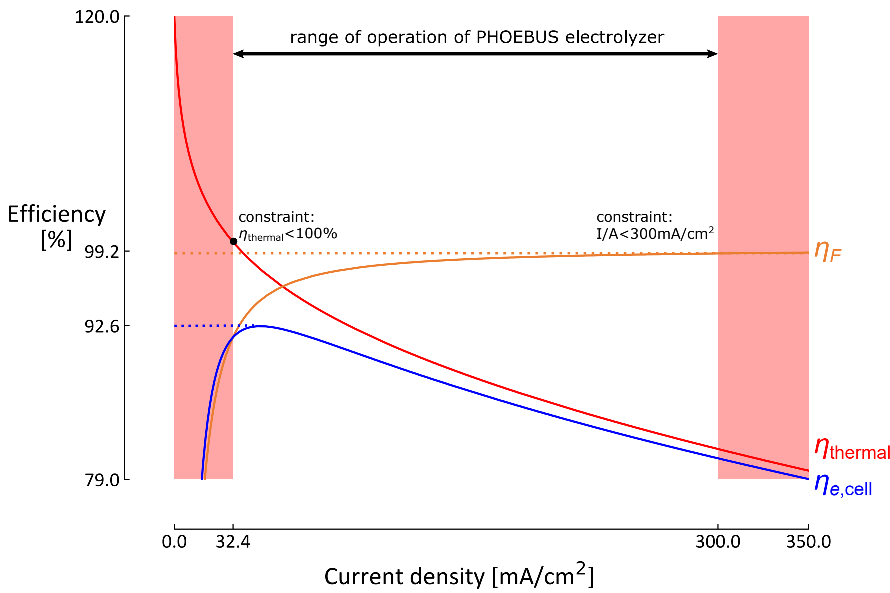

Figure 4: Thermal (η_{thermal}), Faraday (η_{F}) and energy ($\eta_{e,\text{cell}} = \eta_{\text{thermal}}\eta_{\text{F}}$) efficiency of the alkaline electrolyzer in function of the current density at a temperature of 80°C. A peak in the energy efficiency indicates the most optimal point of operation for the electrolyzer to produce H_2. The operational range of the electrolyzer is bounded by a minimum and maximum current density.

The flow towards the Haber-Bosch compressor should consist of a H_2/N_2

ratio between 2 and 3 [39, 42] while the operating pressure lies between 100 and 250 bar [43] (Figure 5). When either of the three parameters of the model exceeds a limit, the to be maximized objectives are penalized with a numerical value of 10^{-9} and the minimized outputs (the CoV in the RDO phase) with 10^{9}. Assigning these numerical values drives the genetic algorithm away from the generated design points and uses the more potent sets of decision variables to evolve towards the best results.

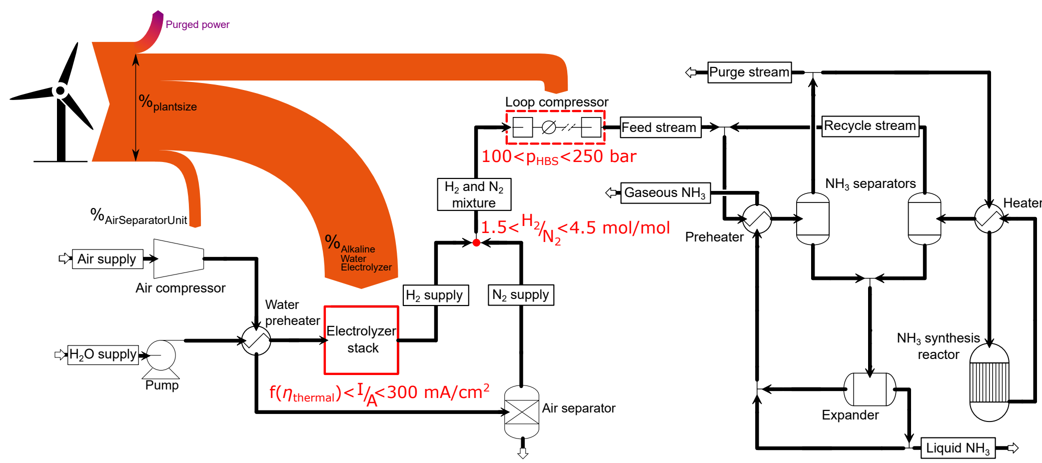

Figure 5: After the optimization algorithm defines the decision variables, a model simulation is executed, and a constraint check is performed to exclude the designs which exceeds one of the imposed constraints, i.e. minimum and maximum current density of the individual alkaline electrolytic cell, the H_2/N_2 ratio or the output pressure of the Haber-Bosch loop compressor.

3.4. Optimization algorithm

To determine the optimal set of design samples for the system model, we implemented the multi-objective Nondominated Sorting Genetic Algorithm (NSGA-II) [27]. First, the algorithm produces an initial set of design samples

(n samples) through Latin Hypercube Sampling [44]. Out of this initial design sample set, the algorithm creates a second sample set based on crossover and mutation, with an equal number of samples n. After characterizing both sets of design samples, each design sample is implemented in the system model and evaluated, leading to $2n$ values for each objective. Thereafter, the samples are sorted based on their dominance on the objectives and the n samples with the highest dominance define the second generation of design samples. This iterative process is repeated until a predetermined number of generations is achieved or the simulation converged towards a solution. Depending on the relation between the multiple objectives, the optimal set of design samples can converge to a single optimal design sample (i.e. non-conflicting objectives) or a set of design samples (i.e. conflicting objectives). In such a set of optimal design samples, each sample dominates every other sample in at least one objective (i.e. Pareto frontier).

3.5. Uncertainty quantification method

To propagate the uncertainties of the input parameters through the system model, we implemented the Polynomial Chaos Expansion (PCE) algorithm [45, 46]. This technique provides a computationally efficient alternative for the robust Monte Carlo Simulation technique for a small stochastic dimension (< 10). To quantify the mean and standard deviation of the objective efficiently, the PCE algorithm creates a surrogate model $\hat{M}(\boldsymbol{\xi})$ of the physical model $M(\boldsymbol{\xi})$ based on multivariate orthogonal polynomials Ψ_i and corresponding coefficients u_i:

$$\hat{M}(\boldsymbol{\xi}) = \sum_{i=0}^{P} u_i \Psi_i(\boldsymbol{\xi}) \approx M(\boldsymbol{\xi}). \tag{11}$$

When P in Equation 11 is infinite, the surrogate model is an exact representation of the physical model. In practice, the series is truncated up to a value depending on the complexity of the input-output relation (related to the polynomial order p) and the stochastic dimension d [28]:

$$P + 1 = \frac{(p+d)!}{p!d!}. \tag{12}$$

When the PCE surrogate model is constructed, the mean μ and standard deviation σ follow analytically out of the coefficients:

$$\mu = u_0, \tag{13}$$

$$\sigma^2 = \sum_{i=1}^{P} u_i^2. \tag{14}$$

Next to the statistical moments of the objective, the contribution of each input parameter to the objective variation can be quantified through Sobol' indices. The first-order Sobol' indices (i.e. no input parameter interaction considered) are defined as:

$$S_i = \frac{D_i}{D} = \frac{\mathrm{Var}[M(\xi_i)]}{\mathrm{Var}[M(\boldsymbol{\xi})]}. \tag{15}$$

Similar to the mean and standard deviation, these first-order Sobol' indices can be quantified analytically via the PCE coefficients:

$$S_i^{PC} = \sum_{\alpha \in A_i} u_\alpha / D \qquad A_i = \alpha \in A : \alpha_i = 0, \alpha_{j \neq i} = 0. \tag{16}$$

4. Results and discussion

This section presents the results and discussion of the DDO and RDO approaches, applied to the power-to-ammonia energy storage system. A global sensitivity analysis applied to the DDO results shows the effect of the uncertainties on the performance of two deterministic optimums. To minimize the effect of the uncertainties on the performance, the RDO approach takes them into account and find a design that can minimize their effects on these results. Again, a global sensitivity analysis is performed on the most relevant designs to show which uncertainties have the most impact on the robustified designs. Finally, we proposed different measures to further reduce the effect of these uncertainties on the RDO results.

4.1. Deterministic design optimization

The deterministic design optimization with a population (n) of 24 samples resulted in a collection of optimized solutions when maximizing the annual NH_3 production and the plants' load factor. The NSGA-II algorithm converged to this set of solutions −or Pareto points− after 33 iterations due to the conflicting objectives: maximizing $m_{\mathrm{NH_3,total}}$ and L_F. This Pareto front consists of two designs, each configured with two unique decision variables, which enables the optimized performance for a particular objective (Table 3). These two extreme cases are named 'Most NH_3' and 'Best L_F'. Each intermediate set of decision variables between those extremities provides a combination of maximizing both output objectives with a certain weight. The results of the UQ analysis on the two cases show the dominance of the wind speed measurement and the ammonia reactor temperature (Figure 6).

Table 3: Set of decision variables and results of the two extremities of the Pareto front. An increase in the NH_3 plant size ($\%_{\text{plantsize}}$) increases the amount of electrolyzers (N) and the power distribution to the AWE ($\%_{\text{AWE}}$). This small increase in power distribution to the AWE relates to the non-linear behavior of the electrolyzer model.

Decision variable		Case	
		Most NH_3	Best L_F
$\%_{\text{plantsize}}$	[%]	92.4	6.58
N	[-]	2500	954
$\%_{\text{AWE}}$	[%]	91.8	91.6
$\%_{\text{PSA}}$	[%]	1.60	1.60
Result			
$m_{NH_3,\text{total}}$	[tonne]	491	122
L_F	[%]	22.4	73.5

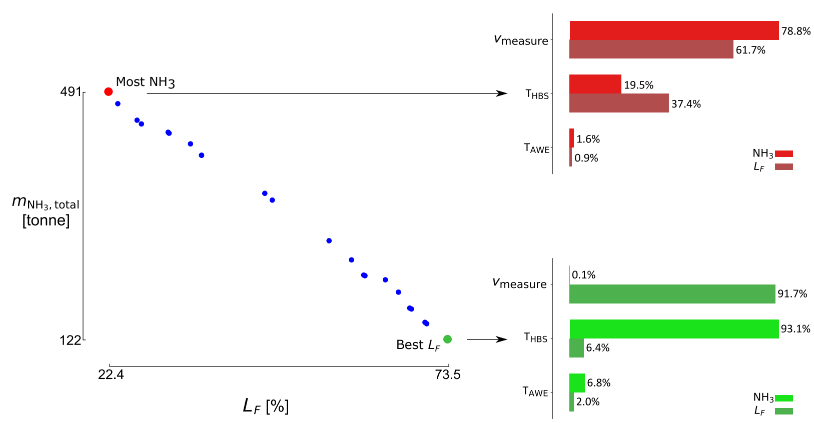

Figure 6: The DDO algorithm provided a design trade-off when maximizing the annual NH_3 production and the load factor (L_F). A global sensitivity analysis shows the dominance of the wind speed measurement influencing the load factor and the NH_3 production in the 'Most NH_3' design. In the best L_F design, the reactor temperature dominates the NH_3 production.

The 'Most NH_3' design enables the highest storage of available wind energy to the energy carrier, ammonia. To obtain this most productive plant, a plant with a load of 2.77 MW (92.4% of the 3 MW WTG capacity) needs to be built, while it needs to be composed of an electrolyzer stack of 2500 individual electrolytic cells. The number of alkaline electrolytic cells prevents the plant to capture the total wind turbine capacity of 3 MW. When the GA generates a larger plant size, and the same number of electrolyzers is incorporated, the plant would be unable to operate at lower wind power due to the minimum current density (Figure 4). This set of decision variables would result in lower annual ammonia production and therefore withdrawn from the set of optimal decision variables. The plant achieves a load factor of 22.4%, which results in a low utilization rate of the total plant. However, for this design case, there is a potential to produce a large amount of ammonia that variates instantaneously with the wind speed. This would be an ideal way to capture the excessive power from the WTG. However, a commercial ammonia synthesis design is not adapted to this flexible functioning [9]. The observed pressure variations are problematic, knowing that the ramp-up of the process is time-constrained (multiple hours to ramp-up the ammonia production) [23]. This could, although, be solved by accumulating hydrogen and nitrogen gas in storage tanks before the synthesis loop while supplying a constant mass flow of the mixture to the Haber-Bosch process. This makes the system less vulnerable to pressure changes if small fluctuations of power are guaranteed to this part of the plant.

For the design with the highest load factor ($L_F = 73.5\%$), the plant consumes 6.58% of the 3 MW WTG capacity (0.197 MW) while consisting of 954 electrolytic cells. A sensitivity analysis of this design showed that the NSGA-II algorithm established a plant design with a stable ammonia production and an electrolyzer stack performing at the peak energy efficiency of 92.6% (Figure 4). This 'Best L_F' design produces a steady low flow of ammonia, which is almost invulnerable to the variations of wind speed. This design type is the most common way to produce ammonia in combination with a grid connection to compensate for the absence of wind power [43], like the pilot plant in Minnesota [17]. Aside from the stable production, the amount of potential wind power discarded from the simulation (73.4% of the residual wind power) is unwanted when the principal use is equalizing the supply and demand of the electric grid. Complementary to the Haber-Bosch plant, the consumption of this residual excess energy, in this case, provides the necessity to install other flexible storage systems.

A global sensitivity analysis showed the effect of uncertainties applied to the two extreme cases, together with the corresponding Sobol' indices (Figure 6). The UQ analysis provided a mean value for both objectives, which was lower than their deterministic counterparts due to the adverse effect of the uncertainties on the total performance. The analysis applied on the 'Most NH_3' design resulted in a relative decrease of 0.62% in the ammonia production ($\mu_{\mathrm{NH_3,total}} = 488$ tonne NH_3) and a relative decrease in load factor by 6.63% ($\mu_{L_F} = 20.9\%$). The CoV of the NH_3 production and the load factor of the plant for the 'Most NH_3' case are respectively 1.57% and 7.46%. This result subsequently indicates that the load factor of this design is more affected by the variations of the uncertain parameters than the ammonia production. The UQ analysis of the 'Best L_F' design presented a relative decrease of 0.56% in NH_3 production and 0.03% for L_F between the mean and the deterministic result, where the CoV of both outcomes, in this case, are respectively 0.70% and 0.07%. These values show that the set of optimized decision variables for the best load factor design from the DDO analysis provides an ammonia plant that is insensitive to variations.

Regarding the Sobol' indices, the global sensitivity analysis shows the noise propagation due to the temperature variations in the NH_3 reactor and the electrolytic cell, and the wind speed measurement error in the two cases for each objective (Figure 6). The temperature variations in the electrolyzer have, in general, less effect on the overall variance of the objective (maximum 6.8% of the total variance in the 'Best L_F' design).

Different operational uncertainties influence the ammonia production in the two extreme cases (Figure 6). In the 'Most NH_3' case, the wind speed measurement error has a more significant effect on the noise propagation of the NH_3 production (78.8%) than in the 'Best L_F' case (0.1%). The influence arises from the fact that the wind speed affects the generated power of the WTG, hence the consumed power by the ammonia plant. This correlation makes the design with the largest ammonia production capacity (consuming 92.4% of the WTG maximum power) more dependable on the wind speed and its parameter variations. On the contrary, for the 'Best L_F' case, this design is only using 6.58% of the WTG maximum power production, which results in a lower annual ammonia yield, but a higher resistance against wind speed measurement errors. However, the reactor temperature variations in this design dominate the ammonia production (93.1%), while this uncertainty influences the result in the other case with only 19.5% of the total variance.

This variation impacts the NH_3 production because of its effect on the equilibrium conditions in the ammonia reactor; directly controlling the amount of ammonia that is produced. The absence of the wind speed measurement error results from the objective to attain a high load factor, which ensures the continuous power flow to the plant; consequently minimizing the effect of the wind speed variation on the NH_3 production. Because the influence of the wind speed is absent in the 'Best L_F' design, this temperature variation will take over the dominant role of the most significant contribution to the variation of the annual ammonia production.

In the case of the load factor, the global sensitivity analysis shows that the wind speed variation has the most considerable contributions in both cases. This equivalent influence emerges with the definition of the load factor as the second optimization objective (Equation 8).

4.2. Robust design optimization

In the interest to find a design that enables the storage of wind power by the production of ammonia while minimizing the impact of the uncertainties on this production, a Robust Design Optimization (RDO) was performed on the model. Combining the NSGA-II algorithm and the PCE method provides a strategy to inexpensively measure the sensitivity of the outcome −or CoV− and progress towards a better set of decision variables, acquired by the GA with a population size (n) of 24 samples in each iteration [46–48]. This approach optimized the wind-powered ammonia synthesis model to determine a design that maximizes the mean NH_3 production while minimizing the CoV of this production.

Similar to the DDO results, the RDO algorithm converged after 25 itera-

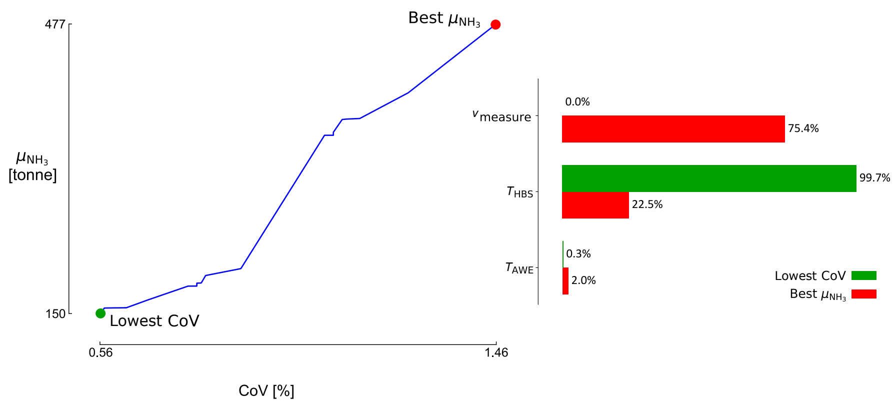

Figure 7: The RDO algorithm provided a design trade-off when maximizing the average NH_3 production and minimizing the Coefficient of Variance (CoV). In the 'Best CoV' case, the temperature variation dominates this average NH_3 production, while the wind speed variations dominate this production for the 'Best μ_{NH_3}' design.

tions to a trade-off between the two chosen objectives, where two extremities each secure a unique set of decision variables to reach a specific objective (Figure 7). In the most robust case ('Lowest CoV'), the energy storage system produces on average low quantities of ammonia (150 tonne of NH_3 annually), but consists of a CoV which is 2.6 times lower than the conflicting optimized design. This conflicting case ('Best μ_{NH_3}') delivers a 3.18 times higher mean production (477 tonne of NH_3 on average) than the 'Lowest CoV' design. These two opposing designs have a key decision variable that determines this difference in production, namely the fraction of power allowed from the 3 MW wind turbine (i.e. the power plant size). This crucial decision variable creates this trade-off of robustification (Table 4). In comparison with the obtained DDO decision variables (Table 3), the RDO decision variables have a similar design configuration with the 'Most NH_3' case of the DDO process. This shows that the exploration and exploitation of the Latin Hypercube and NSGA-II algorithm reach the same results for the same objective in the different optimization cases. The Gaussian uncertainties cause different ammonia productions.

Table 4: Set of decision variables (number of electrolyzer cells, power allocation to the main and subprocesses) generated by the NSGA-II algorithm and results of the two extremities ('Best μ_{NH_3}' and 'Lowest CoV') from the Pareto front established by the RDO process. The NH_3 plant size ($\%_{plantsize}$) is the key decision variable for composing a robust ammonia plant.

Decision variable		Case	
		Best μ_{NH_3}	Lowest CoV
$\%_{plantsize}$	[%]	85.7	11.4
N	[-]	2490	2339
$\%_{AWE}$	[%]	91.9	92.5
$\%_{PSA}$	[%]	1.59	1.23
Result			
μ_{NH_3}	[tonne]	477	150
CoV	[%]	1.46	0.56

A global sensitivity analysis of the NH_3 production applied on the two extreme trade-off designs resulted in the individual variance of each operational uncertainty presented through the Sobol' indices (Figure 7). According to these Sobol' indices, a different operational uncertainty influences the ammonia production of the two designs. In the 'Lowest CoV' (most robust) design case, the temperature variations of the ammonia reactor dominate these results. This influence was also observed in the DDO results with the 'Best L_F' design, where the effect of the wind speed measurement error was (almost) nullified by changing the size of the ammonia plant (decision variable $\%_{\text{plantsize}}$). This results that the residual two uncertainties (T_{HBS} and T_{AWE}) influence the average ammonia production. The temperature of the ammonia reactor has a direct effect on the ammonia production, which accounts for having the most significant impact on the sensitivity of the ammonia production (Figure 7). If the objective is to create a robust ammonia plant, the temperature variations of the reactor need to be smaller. Jinasena et al. already provided examples on how to stabilize temperature fluctuations by increasing the monitoring measurements of the heat exchanger that controls the incoming flow. These measurements consisted of analyzing the composition of feed gases, feed flow rate, reactor inlet temperature and the pressure along the reactor [40]. In the other case ('Best μ_{NH_3}'), a plant design is obtained with a CoV of 1.46% and an annual mean ammonia production of 477 tonne which is mostly influenced by the wind speed measurement error and (in smaller quantities) the temperature of the HBS reactor. Like in the 'Most NH_3' case of the DDO, this influence is directly linked to the sizing of the ammonia plant, where a large plant is subjected to wind speed fluctuations and therefore to the wind speed measurement errors. This relationship gives rise to a plant with high annual average ammonia production, but more sensitive to the wind speed measurement error than the robust design. The impact of the accuracy of the wind speed can be reduced by implementing a more accurate wind speed measurement device and a better calibration/positioning of the anemometer. As in the deterministic optimization, the temperature variations of the AWE have little effect on the performance of the ammonia plant, although 91.9% of the consumed power goes to the alkaline electrolyzer for the production of H_2.

5. Conclusion

This paper provided the steady-state modeling and optimization of an NH_3-based energy storage system in Aspen Plus based on the expected wind power production from a designed WTG in Python. The integrated WTG powered the AWE, PSA and HBS compressor in a certain ratio, so the storage of wind energy through ammonia production could be optimized by the applied multi-objective optimization approach, i.e. the NSGA-II algorithm. Adjacent to the modeling of these subsystems, we identified and integrated the wind speed measurement error, the temperature variation of the electrolyzer and the NH_3 synthesis reactor as the operational uncertainties. The PCE algorithm measured the uncertainty propagation of these operational uncertainties when analyzing a certain objective. The multi-objective DDO consisted of maximizing the ammonia production and the plants' load factor with the NSGA-II algorithm. In the RDO step, the optimization and robustification of this ammonia production was requested from the NSGA-II algorithm in combination with the PCE method.

The DDO step provided a Pareto front where its outer ends delivered a productive and high load factor design. The power sizing of the storage system and the number of electrolytic cells are the key decision variables allowing a design to capture wind energy or a design able to operate continuously. A global sensitivity analysis on each objective showed that the temperature variations of the ammonia reactor and the wind speed measurement influence the load factor, while the NH_3 production is either dominated by the wind speed measurement or by the temperature fluctuation in the ammonia reactor. The integrated temperature variations in the AWE have little influence on the noise on each DDO objective.

Similar to the DDO case, the robust optimization procedure delivered a trade-off between a productive and a robust design. The key decision variable for obtaining either one of the two designs lies within the sizing of the total storage system. A larger sized storage system grants the opportunity to produce higher amounts of ammonia, but is subjected to the uncertainty of the wind speed measurement and the temperature fluctuation in the ammonia reactor. In contrast to this productive design, the most robust design provides lower quantities of ammonia, but is only subjected to the temperature fluctuation of the ammonia reactor and in smaller proportion to the temperature variation in the AWE. Implementing a more accurate wind speed measurement device and increasing the monitoring measurements of the heat exchanger that controls the incoming flow towards the HBS reactor can decrease the CoV on the NH_3 production in both RDO cases. A future investigation will involve analyzing the dynamic operations of the power-to-ammonia pathway and robustifying its levelized cost.

Acknowledgments

The work has been performed in the scope of the GenComm project, funded by Interreg North-West Europe. Aspen Plus was used under academic license.

Appendix A. Parameters alkaline water electrolyzer

Table A.5: Model parameters of the AWE located in the PHOEBUS plant operating at a pressure of 7 bar and a temperature between 30 and 80°C [36].

U-I parameters		Value
r_1	[Ωm^2]	7.33110^{-5}
r_2	[Ωm^2 °C^{-1}]	-1.1010^{-7}
s_1	[V]	1.58610^{-1}
s_2	[V °C^{-1}]	1.37810^{-3}
s_3	[V °C^{-2}]	-1.60610^{-5}
t_1	[m^{2}A^{-1}]	1.59910^{-2}
t_2	[m^{2}A^{-1} °C^{-1}]	-1.302
t_3	[m^{2}A^{-1} °C^{-2}]	421.310^2
A	[m^2]	0.25
η_F parameters		
f_1	[%]	99.5
f_2	[m^{2}A^{-1}]	-9.5788
f_3	[m^{2}A^{-1} °C^{-1}]	-0.0555
f_4	[m^{4}A^{-1}]	1502.7083
f_5	[m^{4}A^{-1} °C^{-1}]	-70.8005

References

[1] M. Lott, S.-I. Kim, C. Tam, D. Elzinga, S. Heinen, L. Munuera, U. Remme, Technology Roadmap: Energy storage, International Energy Agency (2014) 64.

[2] A. Evans, V. Strezov, T. J. Evans, Assessment of utility energy storage options for increased renewable energy penetration, Renewable and Sustainable Energy Reviews 16 (2012) 4141–4147.

[3] G. Wang, A. Mitsos, W. Marquardt, Conceptual design of ammonia-based energy storage system: System design and time-invariant performance, AIChE Journal 63 (2017) 1620–1637.

[4] F. Díaz-González, A. Sumper, O. Gomis-Bellmunt, R. Villafáfila-Robles, A review of energy storage technologies for wind power applications, Renewable and Sustainable Energy Reviews 16 (2012) 2154–2171.

[5] C. Wulf, J. Linßen, P. Zapp, Review of Power-to-Gas Projects in Europe, Energy Procedia 155 (2018) 367–378.

[6] M. Kopp, D. Coleman, C. Stiller, K. Scheffer, J. Aichinger, B. Scheppat, Energiepark Mainz: Technical and economic analysis of the worldwide largest Power-to-Gas plant with PEM electrolysis, International Journal of Hydrogen Energy 42 (2017) 13311–13320.

[7] G. Guandalini, M. Robinius, T. Grube, S. Campanari, D. Stolten, Long-term power-to-gas potential from wind and solar power: A country analysis for Italy, International Journal of Hydrogen Energy 42 (2017) 13389–13406.

[8] WaterstofNet to lead European hydrogen truck project H2-Share, Fuel Cells Bulletin 2017 (2017) 3.

[9] Institute for Sustainable Process Technology, Power to Ammonia, Technical Report, ISPT, 2017.

[10] U. Bossel, B. Eliasson, Energy and the Hydrogen Economy, ABB Switzerland Ltd (2009) 1–35.

[11] J. Fuhrmann, M. Hülsebrock, U. Krewer, Energy Storage Based on Electrochemical Conversion of Ammonia, in: Transition to Renewable Energy Systems, Wiley-VCH Verlag GmbH & Co. KGaA, Weinheim, Germany, 2013, pp. 691–706.

[12] I. I. Cheema, U. Krewer, Operating envelope of Haber–Bosch process design for power-to-ammonia, RSC Advances 8 (2018) 34926–34936.

[13] E. Morgan, J. Manwell, J. McGowan, Wind-powered ammonia fuel production for remote islands: A case study, Renewable Energy 72 (2014) 51–61.

[14] R. Bañares-Alcántara, G. Dericks III, M. Fiaschetti, P. Grünewald, J. Masa Lopez, E. Tsang, A. Yang, L. Ye, S. Zhao, Analysis of Islanded Ammonia-based Energy Storage Systems, Technical Report, University of Oxford, Oxford, 2015.

[15] D. Frattini, G. Cinti, G. Bidini, U. Desideri, R. Cioffi, E. Jannelli, A system approach in energy evaluation of different renewable energies sources integration in ammonia production plants, Renewable Energy 99 (2016) 472–482.

[16] A. Valera-Medina, H. Xiao, M. Owen-Jones, W. I. David, P. J. Bowen, Ammonia for power, Progress in Energy and Combustion Science 69 (2018) 63–102.

[17] M. Reese, C. Marquart, M. Malmali, K. Wagner, E. Buchanan, A. McCormick, E. L. Cussler, Performance of a Small-Scale Haber Process, Industrial & Engineering Chemistry Research 55 (2016) 3742–3750.

[18] I. Wilkinson, Siemens green Ammonia, 1st NH3 European event, Netherlands: Rotterdam, 2017.

[19] M. Aziz, T. Oda, A. Morihara, T. Kashiwagi, Combined nitrogen production, ammonia synthesis, and power generation for efficient hydrogen storage, Energy Procedia 143 (2017) 674–679.

[20] K. E. Lamb, M. D. Dolan, D. F. Kennedy, Ammonia for hydrogen storage; A review of catalytic ammonia decomposition and hydrogen separation and purification, International Journal of Hydrogen Energy 44 (2019) 3580–3593.

[21] A. Sánchez, M. Martín, Optimal renewable production of ammonia from water and air, Journal of Cleaner Production 178 (2018) 325–342.

[22] A. Sánchez, M. Martín, Scale up and scale down issues of renewable ammonia plants: Towards modular design, Sustainable Production and Consumption 16 (2018) 176–192.

[23] A. Allman, P. Daoutidis, Optimal scheduling for wind-powered ammonia generation: Effects of key design parameters, Chemical Engineering Research and Design 131 (2018) 5–15.

[24] S. Schulte Beerbühl, M. Fröhling, F. Schultmann, Combined scheduling and capacity planning of electricity-based ammonia production to in-

tegrate renewable energies, European Journal of Operational Research 241 (2015) 851–862.

[25] M. J. Palys, A. Kuznetsov, J. Tallaksen, M. Reese, P. Daoutidis, A novel system for ammonia-based sustainable energy and agriculture: Concept and design optimization, Chemical Engineering and Processing - Process Intensification 140 (2019) 11–21.

[26] H. Matsumoto, J. Rahat, Y. Manaka, M. Ishii, T. Nanba, Analysis of Influence of Operating Pressure on Dynamic Behavior of Ammonia Production over Ruthenium Catalyst under High Pressure Condition, 2018.

[27] K. Deb, A. Pratap, S. Agarwal, T. Meyarivan, A fast and elitist multiobjective genetic algorithm: NSGA-II, IEEE Transactions on Evolutionary Computation 6 (2002) 182–197.

[28] S. Abraham, M. Raisee, G. Ghorbaniasl, F. Contino, C. Lacor, A robust and efficient stepwise regression method for building sparse polynomial chaos expansions, Journal of Computational Physics 332 (2017) 461–474.

[29] sotaventfogalicia.com, Real time data, 2018. [Online]. Available: `https://bit.ly/2Ezo4F6`. [Accessed: 2 May 2018].

[30] Wind-turbine-models.com, Vestas V112 onshore wind turbine, 2018. URL: `https://bit.ly/2M9xCwL`.

[31] E. I. Kaganov, A. M. Yaglom, Errors in wind-speed measurements by rotation anemometers, Boundary-Layer Meteorology 10 (1976) 15–34.

[32] N. Boccard, Capacity factor of wind power realized values vs. estimates, Energy Policy 37 (2009) 2679–2688.

[33] M. A. Lackner, A. L. Rogers, J. F. Manwell, Uncertainty Analysis in MCP-Based Wind Resource Assessment and Energy Production Estimation, Journal of Solar Energy Engineering 130 (2008) 031006.

[34] A. Buttler, H. Spliethoff, Current status of water electrolysis for energy storage, grid balancing and sector coupling via power-to-gas and power-to-liquids: A review, Renewable and Sustainable Energy Reviews (2017).

[35] J. Proost, State-of-the art CAPEX data for water electrolysers, and their impact on renewable hydrogen price settings, International Journal of Hydrogen Energy (2018).

[36] Ø. Ulleberg, Stand-alone power systems for the future: optimal design, operation & control of solar-hydrogen energy systems, NTNU, Trondheim, Norvège (1998).

[37] M. Mori, T. Mržljak, B. Drobnič, M. Sekavčnik, Integral characteristics of hydrogen production in alkaline electrolysers, Strojniski Vestnik/Journal of Mechanical Engineering 59 (2013) 585–594.

[38] B. Fastrup, H. Nygård Nielsen, On the influence of oxygen on iron catalysts during ammonia synthesis and catalyst characterization, Catalysis Letters 14 (1992) 233–239.

[39] E. R. Morgan, Techno-Economic Feasibility Study of Ammonia Plants Powered by Offshore Wind, Ph.D. thesis, 2013.

[40] A. Jinasena, B. Lie, B. Glemmestad, Dynamic Model of an Ammonia Synthesis Reactor based on Open Information, in: Proceedings of The 9th EUROSIM Congress on Modelling and Simulation, EUROSIM 2016, The 57th SIMS Conference on Simulation and Modelling SIMS 2016, volume 142, 2018, pp. 998–1004.

[41] M. S. Mudahar, T. P. Hignett, Energy efficiency in nitrogen fertilizer production, Energy in Agriculture 4 (1985) 159–177.

[42] L. Tock, F. Maréchal, M. Perrenoud, Thermo-environomic evaluation of the ammonia production, The Canadian Journal of Chemical Engineering 93 (2015) 356–362.

[43] C. Philibert, Producing ammonia and fertilizers: new opportunities from renewables (2017).

[44] M. Stein, Large sample properties of simulations using latin hypercube sampling, Technometrics 29 (1987) 143–151.

[45] B. Sudret, Polynomial chaos expansions and stochastic finite-element methods, 2003, 2014.

[46] D. Coppitters, W. De Paepe, F. Contino, Surrogate-assisted robust design optimization and global sensitivity analysis of a directly coupled photovoltaic-electrolyzer system under techno-economic uncertainty, Applied Energy 248 (2019) 310–320.

[47] P. Tsirikoglou, S. Abraham, F. Contino, Ö. Bağci, J. Vierendeels, G. Ghorbaniasl, Comparison of metaheuristics algorithms on robust

design optimization of a plain-fin-tube heat exchanger, in: 18th AIAA/ISSMO Multidisciplinary Analysis and Optimization Conference, American Institute of Aeronautics and Astronautics, Reston, Virginia, 2017.

[48] W. D. Paepe, D. Coppitters, S. Abraham, P. Tsirikoglou, G. Ghorbaniasl, F. Contino, Robust Operational Optimization of a Typical micro Gas Turbine, Energy Procedia 158 (2019) 5795–5803.